Polymer 104 (2016) 22–30

Contents lists available at ScienceDirect

Polymer

journal homepage: www.elsevier.com/locate/polymer

Nanocellular polymer foams nucleated by core-shell nanoparticles

Shanqiu Liu [a], Bram Zoetebier [a], Lars Hulsman [a], Yuanyuan Zhang [a], Joost Duvigneau [a, b, *], G. Julius Vancso [a, **]

[a] Materials Science and Technology of Polymers, MESA+ Institute for Nanotechnology, University of Twente, P.O. Box 217, 7500 AE, Enschede, The Netherlands
[b] Aerotech Development BV, Drienerlolaan 5, 7522 NB, Enschede, The Netherlands

ARTICLE INFO

Article history:
Received 10 May 2016
Received in revised form
29 July 2016
Accepted 6 September 2016
Available online 8 September 2016

Keywords:
Core-shell nanoparticles
Nanocellular foams
Heterogeneous nucleation efficiency

ABSTRACT

The synthesis of low surface energy polymer grafted silica nanoparticles is reported for the utilization as highly efficient cell nucleation agents to obtain nanocellular, CO_2 blown polystyrene (PS) and poly(-methyl methacrylate) (PMMA) films in a batch process. For nanoparticle surface functionalization hydroxyl-terminated perfluoropolyether and poly(dimethylsiloxane) (PDMS) were used. Their successful grafting to silica nanoparticles was confirmed by Fourier transform infrared (FTIR) spectroscopy, thermogravimetric analysis (TGA) and transmission electron microscopy (TEM). Following melt blending of the modified silica nanoparticles with PS or PMMA their dispersions were evaluated by scanning electron microscopy (SEM) analyses. We demonstrate that proper selection of the polymer grafts results in nucleation efficiencies of up to approximately 0.5 (*i.e.* 1 foam cell per 2 particles on average), which is the highest value reported so far for nanofillers as nucleation agents. This number was confirmed by the presence of only 2 to 4 nanoparticles per cell in nanocellular PS and PMMA foams containing SiO_2 nanoparticles with a PDMS shell as was observed in cross sectional SEM images. The lowest density foam we obtained (~0.32 g cm^{-3}) had a nanocellular morphology with a cell size and cell density of ~440 nm and 1.85×10^{13} cells cm^{-3}, respectively. It is shown that the use of a low surface energy thin shell around silica nanoparticles is beneficial for cell nucleation compared to untreated particles.

1. Introduction

Low density polymer foams with cell sizes of several hundreds of nanometers or smaller comprise a relatively new class of materials that is considered to be of interest for numerous applications, *e.g.* in lightweight structural supports [1], catalysis [2], thermal insulation [3], sound insulation [4], electromagnetic shielding [5,6] and tissue engineering [7]. For instance, Miller and coworkers [8] reported that the confinement of polymer chains in cell walls of nanocellular polyetherimide (PEI) foams leads to a significant increase of toughness and strain at break compared to the microporous material. This enables utilization as lightweight structural support. In addition, when cell diameters are close to, or smaller than, the collision mean free path of gas molecules making up air between successive impacts (~70 nm at standard conditions) [9], the gas phase thermal conduction is minimized. This so called Knudsen effect renders nanocellular polymer foams very promising candidates as high performance thermal insulation materials [10,11]. For instance, Sundarram and coworkers reported a value of 15 mW m^{-1} K^{-1} for the thermal conductivity of a nanocellular polyetherimide foam with a cell size and porosity of 86 nm and 80%, respectively. Despite the rather high polyetherimide foam density the thermal conductivity value for the nanocellular foam reported was significantly lower compared to that of conventional polyurethane based foams (20–22 mW m^{-1} K^{-1}) [12].

For the applications mentioned, control over the foam bulk density is as important as having a nanocellular morphology [13]. Among the possible foaming strategies usually employed, CO_2 assisted batch foaming is frequently used for the preparation of nanoporous foams [14–19]. This is mainly ascribed to CO_2 being considered as a green alternative to other blowing agents. A further advantage is the easy adaptation of batch foaming conditions over a wide pressure and temperature range [20]. Unfortunately, due to

* Corresponding author. Materials Science and Technology of Polymers, MESA+ Institute for Nanotechnology, University of Twente, P.O. Box 217, 7500 AE, Enschede, The Netherlands.
** Corresponding author.
E-mail addresses: j.duvigneau@utwente.nl (J. Duvigneau), g.j.vancso@utwente.nl (G.J. Vancso).

http://dx.doi.org/10.1016/j.polymer.2016.09.016
0032-3861/

size limitations, batch foaming still remains a laboratory scale process [21]. It is foreseen that in the near future novel foaming concepts will be developed that will allow the upscaling of nanocellular foam production to technologically relevant levels.

The majority of the batch foamed nanocellular materials reported in the open literature had foam thicknesses restricted to below a millimeter. In addition, the foams typically had relatively low porosities, *i.e.* below 80%. It was only recently that Costeux and coworkers [13] reported the batch foaming of PMMA copolymers with thicknesses exceeding a few millimeters and a maximum porosity of 85%. However, the production of low density nanocellular polymer foams remains a challenge due to *i*) low cell nucleation numbers, *ii*) fast diffusion of CO_2 out of the foaming polymer and *iii*) coalescence of cells during foaming.

In order to enhance cell nucleation to levels exceeding 10^{14} cells cm^{-3}, the introduction of nanostructured phases to polymers prior to foaming is considered a promising approach. According to the classical nucleation theory (CNT) [22,23] heterogeneous nucleation is preferred over homogeneous nucleation once the interfacial energy and domain size of the heterogeneous phase are properly selected. For instance, foaming of block copolymer blends [24–27] and nanocomposites [13,17,28–36] have been reported.

Nano-clay and silica nanoparticles are among the most widely used heterogeneous nucleation agents [33,34,37]. For example, He and coworkers [33] reported that the addition of nanosilica to polycarbonate prior to batch foaming significantly decreases the foam cell size and increases the cell density compared to neat polycarbonate foams. Ozisik and coworkers [34] described that fluorinated silane modified silica nanoparticles reduced the nucleation free energy barrier and increased the cell density of PMMA foams compared to foams containing pristine silica nanoparticles.

Despite effectively increasing the cell density of polymer foams upon the addition of (modified) nanoparticles, a closer examination of their nucleation efficiency shows that nanoparticles are still often poor nucleation agents. The nucleation efficiency is defined as the ratio of the number of cells per cm^3 of unfoamed material to the number of nanoparticles per cm^3 unfoamed material [29]. This definition, as it is obvious, incorporates cell coalescence and cell collapse. Table 1 shows for a number of selected polymer nanoparticle systems the calculated nucleation efficiencies. Obviously the nucleation efficiency is often orders of magnitude below unity. In the best case the nucleation efficiency was 0.1, meaning that for every 10 particles added 1 cell was nucleated.

In order to enhance the nucleation efficiency of silica nanoparticles Yang and coworkers [38] reported on the grafting of highly CO_2-philic poly(ionic liquid) from silica nanoparticles as nucleation agents for the foaming of microcellular polystyrene foams. Surface initiated atom-transfer radical polymerization (SI-ATRP) was used to graft poly[2-(methacryloyloxy)ethyl]trimethylammonium tetrafluoroborate (P[MATMA][BF_4]) from silica nanoparticle surfaces. Grafted layers with thicknesses of several tens of nanometer were achieved. The authors demonstrated that the CO_2 solubility was slightly enhanced due to the presence of the surface confined P[MATMA][BF_4] phase. Compared to microcellular polystyrene foams prepared with bare silica nanoparticles the cell density increased (factor ~5) and the cell size decreased (factor ~2). However, the overall nucleation efficiency of these polymer decorated nanoparticles remained poor ($<1.7 \times 10^{-3}$).

In this work, we employed a simple "grafting to" approach of low molar mass CO_2-philic and low surface energy polymers on silica nanoparticles in order to have a thin, low surface energy shell around the silica nanoparticles. We explored the nucleation efficiency and foam morphology of the resulting materials. PDMS (19.8 mJ m^{-2}) and Fluorolink E10, *i.e.* a hydroxyl-terminated perfluoropolyether, (18.0 mJ m^{-2}) were selected as the matrix polymers due to their known low surface energy and good wetting property with CO_2 [34,40,41]. For comparison, PS grafted nanoparticles were also synthesized. The core-shell nanoparticles obtained were used as highly efficient heterogeneous nucleation agents for the CO_2 batch foaming of PS and PMMA. We report on substantial enhancement of heterogeneous nucleation efficiency values of up to 0.5.

Table 1
Overview of the (calculated) nucleation efficiency of different polymer/nanofiller systems selected from the literature.

Nanocomposites	Nucleation efficiency
Polypropylene/nanoclay [28]	$<1.0 \times 10^{-4}$
PMMA/nanoclay [17]	$<1.0 \times 10^{-4}$
PS/nanoclay [17]	$<1.0 \times 10^{-4}$
PS/nanoclay [35]	7.4×10^{-4}
PMMA-co-EA/SiO_2 [13]	0.1
PMMA/SiO_2 [13]	4.8×10^{-3}
PMMA/SiO_2 [31]	2.8×10^{-4}
PMMA/fluorinated silane modified SiO_2 [34]	1.5×10^{-4}
PMMA/hydroxyl-terminated SiO_2 [35]	8.6×10^{-6}
Polycarbonate/SiO_2 [33]	1.8×10^{-2}
PS/carbon nanofibers [29]	2.0×10^{-2}
PS/carbon nanotubes [29]	9.1×10^{-5}
PS/amino-terminated SiO_2 [38]	$<3 \times 10^{-4}$
PS/SiO_2 with poly(ionic liquid) grafts [38]	$<1.7 \times 10^{-3}$
PS/SiO_2 with PS grafts [39]	$<2.0 \times 10^{-2}$

2. Experimental section

2.1. Materials

Tetraethyl orthosilicate (TEOS) ≥ 99.0%, (3-aminopropyl)-trimethoxysilane (APTMS) 97%, 2-propanol 99.5%, copper(I) bromide 98% and polystyrene ($M_w = 230{,}000$ g mol^{-1}, $\rho = 1.05$ g cm^{-3}) were purchased from Aldrich (Milwaukee, WI, USA). Ammonium hydroxide solution 28–30%, triethylamine (TEA) 99.5%, copper(II) bromide 99%, α-bromoisobutyryl bromide ≥ 99%, hydrochloric acid 37%, aluminum oxide (for chromatography), nonafluorobutyl methyl ether ≥99%, hydrofluoric acid (48%) and poly(-dimethylsiloxane) monoglycidyl ether terminated (PDMS-G) (M_w = 1000 g mol^{-1}) were purchased from Sigma-Aldrich (St. Louis, MO, USA). PMMA was a gift from Arkema (VM100, *i.e.* a PMMA-*co*-EA polymer, ρ = 1.18 g cm^{-3}) (La Garenne-Colombes, France). Absolute *N*,*N*-dimethylformamide (DMF) and tetrahydrofuran (THF) were purchased from Biosolve (Valkenswaard, the Netherlands). Ethanol absolute for analysis was purchased from Merck (Darmstadt, Germany). Hydroxyl-terminated perfluoropolyether (Fluorolink E10, M_w = 1700 g mol^{-1}) was a gift from Solvay Solexis (Milan, Italy). *N*,*N*,*N*′,*N*′,*N*″-pentamethyldiethylenetriamine (PMDETA) 98% was purchased from Acros Organics (Geel, Belgium). Styrene was passed through an aluminum oxide column prior to polymerization to remove the inhibitor used. Copper(I) bromide was purified by stirring appropriate amounts in water free acetic acid for 24 h, followed by filtration, washing with ethanol for three times and subsequent vacuum drying for at least 12 h. Milli-Q water was produced by a Millipore Synergy system (Billerica, MA, USA). Unless otherwise mentioned all other chemicals were used as received.

2.2. Methods

2.2.1. Silica nanoparticle preparation by the Stöber method, hydrolysis and APTMS functionalization

Stöber-type silica nanoparticles: to prepare Stöber silica

nanoparticles (SiO_2) with a diameter of ~80 nm, 168 ml ethanol was mixed with 28 ml Milli-Q water and 30 ml TEOS in the presence of 2 ml ammonium hydroxide while stirring at 500 rpm at room temperature. After 1.5 h the obtained SiO_2 dispersion was centrifuged at 10,000 rpm for 30 min. Subsequently the collected SiO_2 were redispersed in 2-propanol and centrifuged again. This washing step was repeated 2 more times followed by vacuum drying of the SiO_2 nanoparticles collected, at room temperature for 12 h. Silica particles with a diameter of 120 nm were prepared as described in the supporting information.

Hydrolysis: to introduce silanol groups on the surface of the SiO_2 nanoparticles, the particles were redispersed in Milli-Q water by sonication (BRANSON 2510, Canada) for 1 h. Subsequently, hydrochloric acid was added to the dispersion while stirring at 500 rpm until the pH of the solution reached a value of approximately 1. After 4 h the dispersion was centrifuged at 10,000 rpm for 30 min. The collected nanoparticles were redispersed in Milli-Q water and centrifuged. This washing step was repeated 2 more times followed by drying the silanol functional nanoparticles (SiO_2—OH) in vacuum at room temperature for 12 h.

APTMS modification: 3.0 g SiO_2—OH nanoparticles were redispersed in 100 ml ethanol followed by the addition of 15 ml APTMS. The dispersion was stirred at 500 rpm at room temperature for 17 h. The APTMS functionalized nanoparticles (SiO_2—NH_2) were collected by centrifugation at 10,000 rpm for 30 min and redispersed in ethanol and centrifuged again. This washing step was repeated 2 more times followed by drying the collected SiO_2—NH_2 nanoparticles in vacuum at room temperature for 12 h.

2.2.2. "Grafting to" of the hydroxyl-terminated perfluoropolyether Fluorolink E10 and PDMS-G to silica nanoparticles

Fluorolink E10: 1.0 g of SiO_2—OH nanoparticles were redispersed in 15 ml Fluorolink E10 followed by heating the resulting dispersion to 150 °C for 17 h while stirring at 500 rpm. Subsequently, the Fluorolink E10 modified nanoparticles (SiO_2—F) were cooled to room temperature and washed with nonafluorobutyl methyl ether for 1.5 h followed by centrifuged for 30 min at 10,000 rpm. This washing step was repeated 2 more times, followed by vacuum drying the SiO_2—F nanoparticles at 100 °C for 12 h.

PDMS-G: 1.0 g of SiO_2—NH_2 nanoparticles were redispersed in 20.5 ml THF and 15 g PDMS-G while stirring at 500 rpm for 1 h followed by sonication for 1 h. Subsequently, THF was removed by rotary evaporation and the resulting silica nanoparticle dispersion in PDMS-G was immersed in an oil bath thermostated at 80 °C for 17 h. Following cooling to room temperature the reaction mixture was washed with THF and centrifuged at 10,000 rpm for 30 min. This washing step was repeated 2 more times, followed by vacuum drying the PDMS-G grafted silica nanoparticles at room temperature for 12 h.

2.2.3. ATRP initiator immobilization and SI-ATRP of styrene from silica nanoparticles

Initiator immobilization: 1.5 g SiO_2—NH_2 was redispersed in 75 ml DMF by 30 min of sonication. The mixture was cooled down to 0 °C with an ice bath, followed by dropwise addition of 15 ml TEA and 5 ml α-bromoisobutyryl bromide within 30 min while stirring at 700 rpm. The mixture was stirred for 17 h at room temperature, followed by centrifugation at 10,000 rpm for 30 min. The collected particles were redispersed in ethanol and centrifuged again to remove unreacted TEA, α-bromoisobutyryl bromide and the salt formed by TEA and HBr. This washing step was repeated 2 more times, followed by vacuum drying the ATRP initiator functional nanoparticles (SiO_2—Br) at room temperature for 12 h.

SI-ATRP of styrene: 1.0 g of the SiO_2—Br nanoparticles were redispersed in 10 ml DMF by 30 min of sonication. Two other flasks were prepared, one with 156 mg CuBr and 24.3 mg $CuBr_2$ and another one with 16.87 ml DMF, 12.5 ml styrene and 459 μl PMDETA. All three flasks were equipped with magnetic stirrers and sealed with a rubber septum. The flasks were purged with argon for 1 h. Subsequently, the styrene solution was added to the CuBr/$CuBr_2$ mixture, followed by the addition of SiO_2—Br nanoparticle dispersion to the resulting mixture. Subsequently, the reaction flask was submerged into a 90 °C thermostated oil bath and was stirred at 500 rpm for 17 h under Argon atmosphere. To purify the core-shell nanoparticles, the reaction mixture was washed with DMF and centrifuged at 10,000 rpm for 30min. This washing step was repeated 2 more times after which the collected SiO_2-PS was vacuum dried at room temperature for 12 h. In order to determine the molar mass of the PS brushes the SiO_2 core of a ~100 mg sample dispersed in 2 ml THF was etched with HF for overnight followed by drying the residual polymer. Subsequently the molar mass was measured with GPC to be 9.0×10^3 g mol^{-1}.

2.2.4. Nanocomposite film preparation

Nanocomposite preparation: Nanocomposites were prepared by dispersing 4 wt%, based on the bare silica nanoparticle weight, (functional) silica nanoparticles in PS or PMMA using a mini extruder (DSM Xplore, the Netherlands). In a typical procedure a dry blend of nanoparticles and polystyrene was fed to the extruder followed by internal mixing for 3 min. The barrel temperature was set to 155 °C and the screw speed was 100 rpm. Subsequently the polystyrene nanocomposite was collected and left to cool to room temperature.

Film preparation: A hot press (Fortijne, the Netherlands) was used to press ~0.2 mm thick nanocomposite films in a mold (4×3 cm). The press temperature, applied load and press time were 130 °C, 250 kN and 10 min, respectively.

2.2.5. Batch foaming of nanocomposite films

The nanocomposite PS films obtained were saturated with carbon dioxide (55 bar) in an autoclave for 3 h at room temperature followed by rapid depressurization. Subsequently, the PS films were foamed by immersion in a glycerol bath, which was thermostated at 100 °C for 30 s. Next, the samples were quenched to room temperature in a 50: 50 water-ethanol bath followed by immersion in ethanol for 1 h. Finally, the foams were left to dry in air for at least 12 h prior to further analysis. For the foaming of PMMA nanocomposite films a CO_2 saturation pressure and time of 55 bar and 3 h were used, respectively. Following quick depressurization, the polymer films were foamed by immersion in a water bath thermostated at 40 °C for 3 min after which the samples were quenched in an ice bath for 30 min. Finally the samples were left to dry in air for at least 12 h prior to further analysis. The supporting information contains a scheme of the used foaming setup. We note that the foaming conditions reported provided the lowest cell size and highest cell density within a range of foaming temperatures (0 °C—110 °C and times (few seconds to 5 min) and thus they were selected as our standard conditions throughout this work.

2.3. Characterization

2.3.1. Fourier transform infrared (FTIR) spectroscopy

FTIR spectra were collected with a Bruker ALPHA single attenuated total reflection (ATR) FTIR Spectrometer equipped with an ATR single reflection crystal (Bruker Optic GmbH, Ettlingen, Germany). The spectra were collected in the range of 400–4000 cm^{-1} (spectral resolution of 4 cm^{-1}, 1280 scans). Background spectra were recorded against air.

2.3.2. Thermogravimetric analysis (TGA)

The weight loss of the (modified) particles as a function of temperature was measured with a TGA400 (PerkinElmer, Inc., Waltham, MA, USA). A sample weighing ~3 – 6 mg was loaded into the platinum pan and set to 50 °C to stabilize. Subsequently the sample was heated to 900 °C at a heating rate of 20 °C min^{-1}. The applied N_2 flow was 25 ml min^{-1}.

2.3.3. Transmission electron microscopy (TEM)

To investigate the core-shell structure of the functionalized nanoparticles a FEI/Philips CM300 transmission electron microscope (Eindhoven, the Netherlands) was used. Diluted particle dispersions in THF were deposited on the carbon side of a carbon/copper grid (HC200-Cu) (EMS, Germany). Images were obtained in the bright field mode with a 300 kV acceleration voltage.

2.3.4. Scanning electron microscopy (SEM)

To investigate the morphology of the unfoamed/foamed nanocomposite films a high resolution scanning electron microscope (JEOL Field Emission JSM-633OF, JEOL Benelux, Nieuw-Vennep, the Netherlands) was used. The typical electron acceleration voltage used was 5 keV. Prior to analysis the nanocomposite films and foams were freeze fractured after cooling in liquid nitrogen for 5 min and the obtained cross sections were sputter coated (JEOL JFC-1300 Auto Fine Coater, JEOL Benelux, Nieuw-Vennep, the Netherlands) with gold under argon atmosphere for 40 s at a current of 30 mA.

2.3.5. Calculation of cell density

The cell size and cell density were obtained by analyzing the SEM cross sections. Cell density (N_v) of the foams was calculated by Kumar's theoretical approximation [42]. No direct measurements of cell dimensions over the micrograph are required by this method, only the micrograph area (A) and the total number of cells (n) contained therein are measured. Together with the magnification factor of the micrograph (M), N_v can be calculated according to equation (1):

$$N_v = \left[\frac{(nM^2)}{A}\right]^{3/2} \quad (1)$$

By combining N_V with the volume expansion ratio (B) of nanocomposite films after foaming, the cell numbers per cm^3 of unfoamed materials (N) can be calculated according to equation (2).

$$N = N_v{*}B \quad (2)$$

3. Results and discussion

3.1. Preparation and characterization of nanoparticles

Stöber silica nanoparticles were synthesized, followed by their surface grafting with polystyrene, PDMS or Fluorolink E10, respectively. The reaction scheme is depicted in Fig. 1. Silica nanoparticles with a diameter of ~80 nm were prepared via a Stöber reaction (step 1a), followed by the hydrolysis of the surface exposed ethoxy groups to silanol moieties (step 1b). Subsequently, the hydrolyzed particles were modified with APTMS, resulting in the formation of amine functionalized nanoparticles (step 1c). Following the reaction with α-bromoisobutyryl bromide a macroinitiator nanoparticle (step 1d) for the subsequent SI-ATRP of styrene (step 1e) was obtained. PDMS and Fluorolink E10 grafted core-shell structure nanoparticles were synthesized by the “grafting to” approach of PDMS-G (step 1d') and Fluorolink E10 (step 1c') to the amine functionalized and hydrolyzed silica nanoparticles, respectively.

Fig. 2a shows FTIR absorbance spectra of the (modified) silica nanoparticles. The remaining ethoxy groups after the Stöber reaction of TEOS are clearly observed in the FTIR spectra of the SiO_2 particles, *i.e.* the CH_2/CH_3 bending absorption band at 1452 cm^{-1} and CH_2/CH_3 absorption band at 2980 cm^{-1} [43]. After hydrolysis these absorbance bands disappeared (data not shown). The absorption bands at 1452 cm^{-1} (ascribed to C=C stretching vibrations) and near 3000 cm^{-1} (ascribed to aromatic and aliphatic C–H stretching) indicate the successful grafting of PS from silica nanoparticles [39]. The absorption bands for CH_3 stretching at 2967 cm^{-1} and for C–H bending at 1263 cm^{-1} confirm the successful grafting of PDMS to silica nanoparticles [44]. The absorption band at 1180 cm^{-1}, which is ascribed to C–F stretching modes, indicates the successful grafting of Fluorolink E10 to the silica nanoparticles [45].

TGA was used to determine the amount of polymer grafted from/to the SiO_2 nanoparticles. Fig. 2b shows the weight loss versus temperature curves for non-isothermal TGA measurements of SiO_2, SiO_2-PS, SiO_2–F and SiO_2-PDMS. The weight percentage of PS, Fluorolink E10 and PDMS covalently bound to SiO_2 nanoparticles was determined to be 18.4 wt%, 7.8 wt% and 5.0 wt%, respectively, from mass loss values. Based on the TGA results, the molar mass of grafted polymer chains (*i.e.* 9000 g mol^{-1}, 1700 g mol^{-1} and 1000 g mol^{-1} for PS, Fluorolink E10 and PDMS, respectively) and the surface area of the used SiO_2 nanoparticles (33 m^2 g^{-1}), the PS, Fluorolink E10 and PDMS grafting densities were calculated to be 0.45 nm^{-2}, 0.90 nm^{-2} and 0.91 nm^{-2}, respectively.

TEM was used to confirm the core-shell structure of the nanoparticles (see Fig. 3). The value of the bare silica nanoparticle diameter was determined to be 79.0 ± 9.0 nm. A clear core-shell structure is observed for the SiO_2-PS, SiO_2–F and SiO_2-PDMS nanoparticles (see Fig. 3b–d) and the shell thickness was estimated to be 12.5 ± 1.2 nm, 8.0 ± 1.4 nm and 6.0 ± 1.3 nm, respectively. Hence, bare and core-shell nanoparticles were successfully synthesized, and the prepared nanoparticles were used as nucleation agents for nanocomposite foaming (see section 3.2).

3.2. Nanocomposite foams

Prior to foaming the prepared nanoparticles were melt-blended in a PS matrix and pressed to films with a thickness of ~200 μm. The nanoparticle concentration was 4 wt% based on the silica core content. Hence all nanocomposite films had the same particle density prior to foaming. SEM was used to investigate the dispersion of nanoparticles in the respective PS nanocomposites.

Fig. 4 shows SEM images of sections of freeze fractured PS nanocomposite films. It is obvious that SiO_2-PS and SiO_2-PDMS nanoparticles were well dispersed in PS, while some aggregates for SiO_2 and SiO_2–F nanoparticles melt blended in PS were observed. For Fluorolink E10 modified nanoparticles the observed aggregation is ascribed to the bi-functionality of the polymer used in the bulk grafting reaction *i.e.* potentially one chain end reacts with one particle while the other chain end may react with the same, or with a different particle. Hence, although undesirable, some particle aggregation could not be prevented for this type of core-shell nanoparticle.

The PS nanocomposites with different core-shell structured nanoparticles were foamed after saturation with CO_2 at 55 bar. The densities of the PS foams were calculated based on the expansion ratio (see supporting information) and the values obtained are shown in Table 2.

Fig. 5 shows SEM images of sectioned PS foams without and

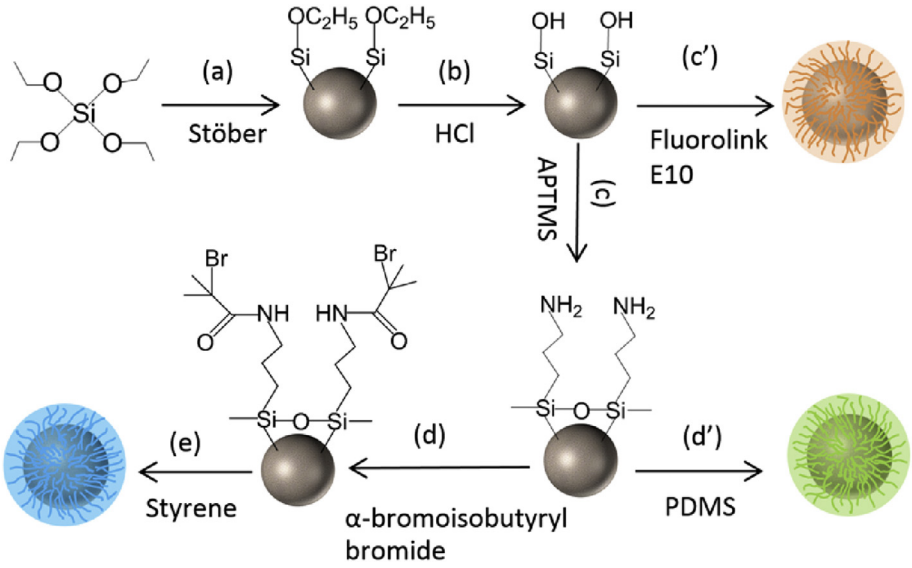

Fig. 1. Particle preparation strategies: Stöber silica nanoparticles were prepared (a) followed by hydrolysis of surface exposed ethoxy groups in diluted HCl (b). Subsequently, amine groups were introduced to the surface of the nanoparticles (c) followed by modification with a bromine terminated ATRP initiator (d) for the SI-ATRP of styrene (e). The grafting to of PDMS and Fluorolink E10 are shown in Fig. 1d' and c', respectively.

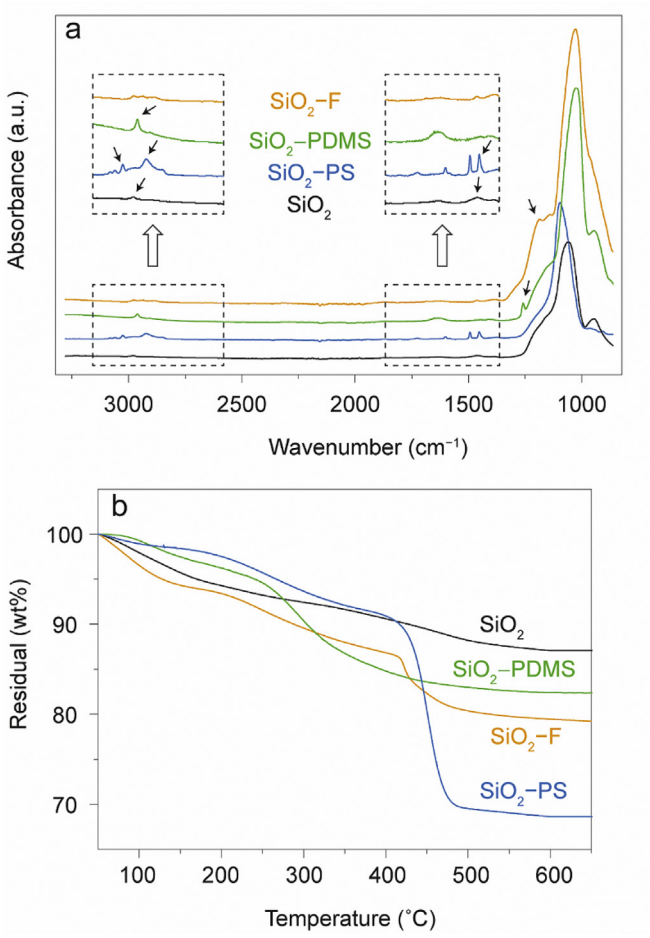

Fig. 2. ATR-FTIR absorbance spectra (a) and non-isothermal TGA thermograms (b) of SiO_2, SiO_2-PS, SiO_2—F and SiO_2-PDMS nanoparticles. In Fig. 2a the black arrows indicate characteristic FTIR absorption bands of the bare and core-shell silica nanoparticles.

with nanoparticles. From Fig. 5 it is obvious that the incorporation of (modified) silica nanoparticles significantly decreases the cell size and increases the cell density. For a good comparison the cell size and cell density of the respective PS foams were determined. The results obtained are shown in Fig. 6.

The average cell size and cell density of neat polystyrene foams were ~2.4 μm and 1.0×10^{11} cells cm^{-3}, respectively (Fig. 6a and b). Upon the addition of 4 wt% bare SiO_2 nanoparticles to PS the cell size decreased to ~1.1 μm and the cell density increased to 1.2×10^{12} cells cm^{-3} (Fig. 6a and b). This is ascribed to heterogeneous cell nucleation at the silica nanoparticle-polymer interface. The cell size and cell density of composites containing SiO_2-PS nanoparticles were ~0.7 μm and 2.5×10^{12} cells cm^{-3}, respectively (Fig. 6a and b). This improvement in foam morphology compared to the bare SiO_2 nanoparticle containing PS foam is explained by the better particle dispersion for the PS grafted SiO_2 particles (compare Fig. 4b and c). This observation is in agreement with results reported by Jingtao and coworkers [39]. They showed that the grafting of PS on mesoporous silica nanoparticles improved the dispersion of the particles as well as the polystyrene foam morphology.

Upon the addition of SiO_2 particles grafted with low surface energy polymers the cell size was further reduced to ~440 nm and the cell density increased to 1.85×10^{13} cells cm^{-3} (Fig. 6a and b). The effect on cell size and cell density was less pronounced for the Fluorolink E10 modified nanoparticles, which we ascribe to the observed particle clustering that reduces the effective number of nucleation sites (see Fig. 4d).

Fig. 6c shows the calculated nucleation efficiencies of the nanoparticles used. Since 4 wt% of nanoparticles was added to the nanocomposites based on their respective silica content, the number of theoretical nucleation sites, *i.e.* 7.5×10^{13} particles per cm^3 of unfoamed material, was the same for all nanocomposites. Hence, this number was used to calculate the nucleation efficiency for each type of particles. In the supporting information the expansion ratios of the obtained foams are shown. These are needed to calculate the number of cells per unit volume of unfoamed material with equation (2).

Obviously, the nucleation efficiency of polymer decorated

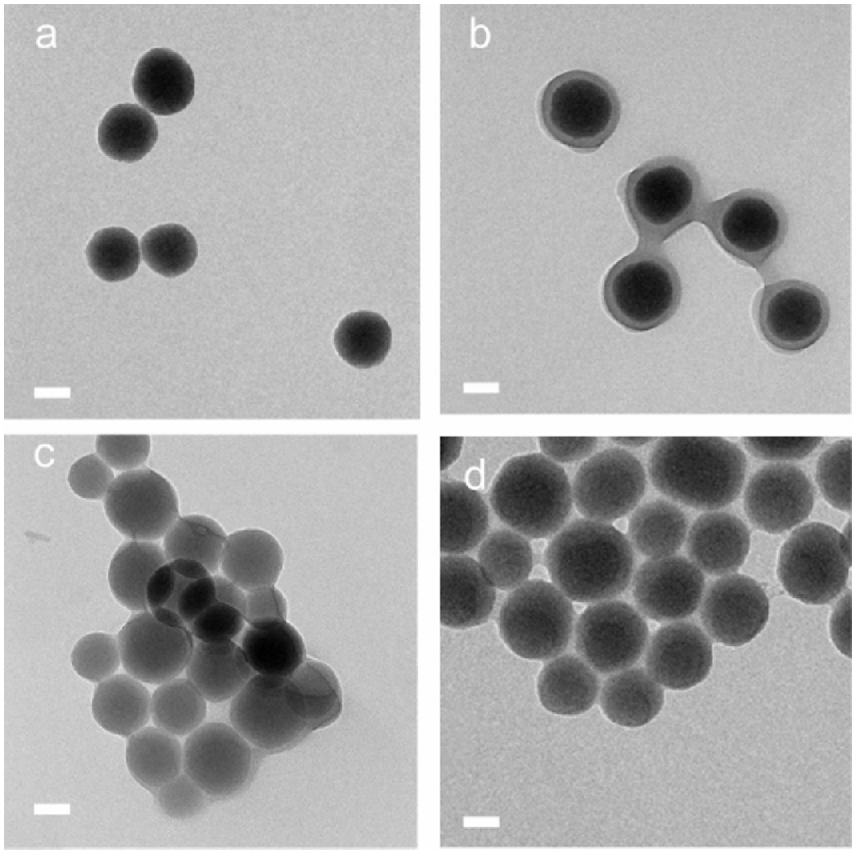

Fig. 3. TEM images of SiO_2 (a), SiO_2-PS (b), SiO_2–F (c) and SiO_2-PDMS (d) nanoparticles. The scale bars represent 50 nm.

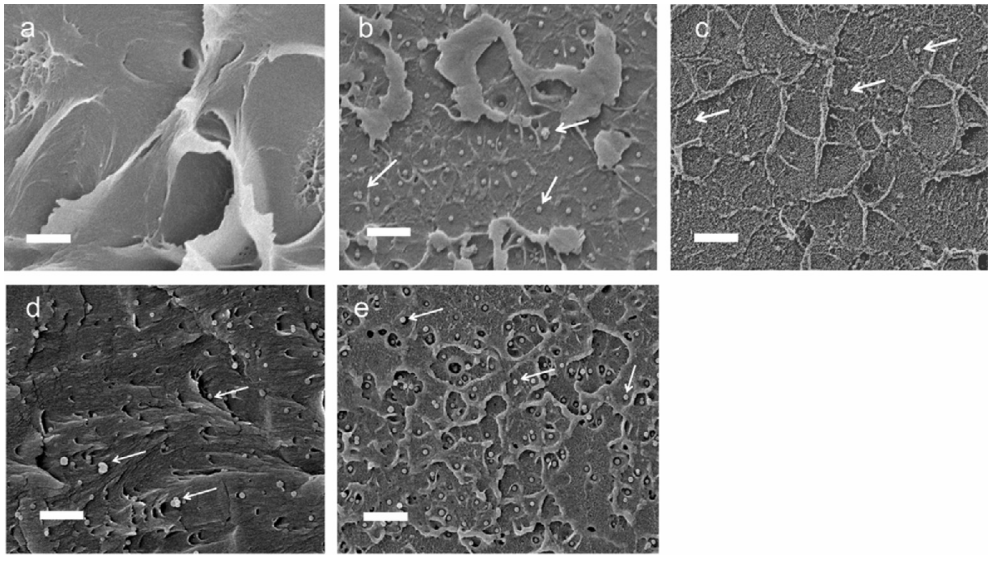

Fig. 4. SEM images of freeze fractured polystyrene films containing no SiO_2 (a), SiO_2 (b), SiO_2-PS (c), SiO_2–F (d) and SiO_2-PDMS (e) nanoparticles. The white arrows point at selected nanoparticles. The scale bars represent 1 μm.

Table 2
Densities of the obtained PS (nanocomposite) foams ($g \cdot cm^{-3}$).

Foam	Neat PS	PS with SiO_2	PS with SiO_2-PS	PS with SiO_2–F	PS with SiO_2-PDMS
Density	0.42	0.46	0.34	0.36	0.32

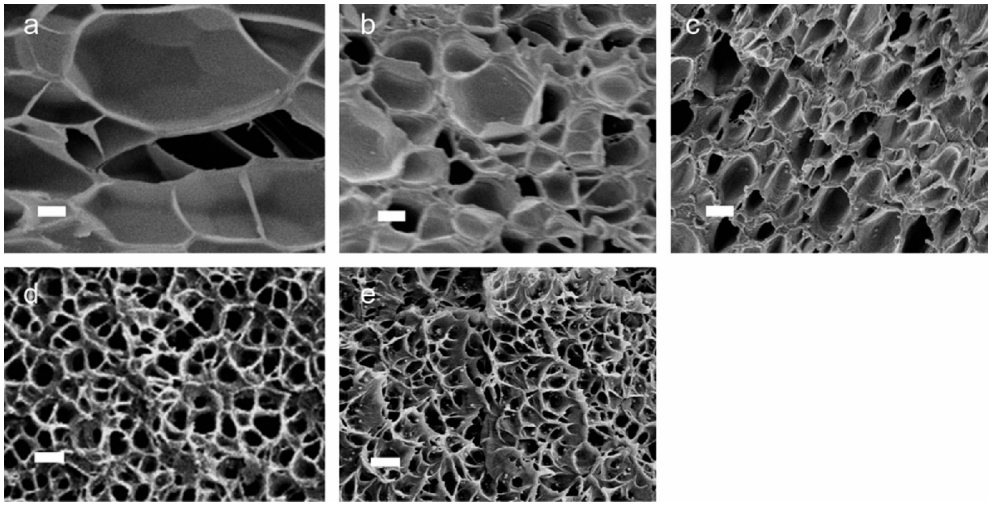

Fig. 5. SEM images of sectioned PS foams containing no SiO_2 (a), SiO_2 (b), SiO_2-PS (c), SiO_2–F (d) and SiO_2-PDMS (e) nanoparticles. The scale bars represent 1 μm. The saturation pressure and foaming temperature were 55 bar and 100 °C, respectively.

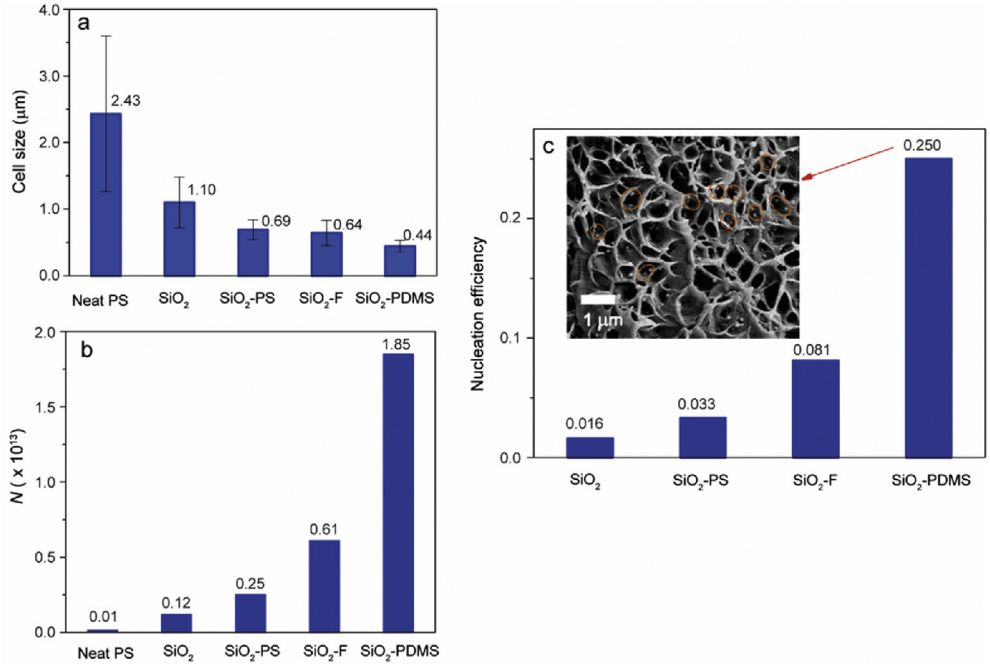

Fig. 6. Cell size (a), cell density (b) and nucleation efficiency (c) of neat polystyrene and polystyrene nanocomposite foams containing SiO_2, SiO_2-PS, SiO_2–F and SiO_2-PDMS nanoparticles.

particles is better compared to the bare silica nanoparticles. The highest nucleation efficiency, *i.e.* 0.25, was obtained for the PDMS grafted SiO_2 nanoparticles. The SEM image in the inset in Fig. 6c shows that for this foam every cell cross section contains about 2 particles. If we assume that on average every cell was cut in half this number is in good agreement with the observed nucleation efficiency, *i.e.* 4 particles result in the formation of 1 cell. The nucleation efficiency of the PDMS coated nanoparticles is 15 times higher compared to the bare silica nanoparticles. In particular these particles perform significantly better compared to the CO_2-philic polyionic liquid grafted nanoparticles reported on by Yang and coworkers [38] (see also Table 1). However direct comparison is not straight-forward since it is known that the foaming conditions (*i.e.*, foaming temperature and saturation pressure) used influence the performance of the nanoparticles added. Despite this, the high nucleation efficiency for the SiO_2-PDMS nanoparticles is ascribed to *i*) the low surface energy of the PDMS shell, *ii)* the higher local CO_2 concentration in the PDMS shell compared to the PS matrix and *iii*) their good dispersion in the PS matrix. In addition, the interfacial interactions between the nanoparticle shell and polymer matrix is expected to affect cell nucleation as well. In fact, it has been reported that for a poor polymer shell matrix interaction the nucleation energy barrier is reduced [27,46]. Studying cell nucleation at the nanometer length scale is highly challenging and currently we are working on establishing methods to quantify the role of the low surface energy shell and the polymer interphase on cell nucleation.

In order to further elucidate the impact of the grafted PDMS coating on nucleation, silica nanoparticles with a diameter of

120 nm and PDMS shells were prepared and melt blended with PMMA at a concentration of 4 wt%. Following CO_2 sorption (55 bar, room temperature, 3 h) the CO_2 saturated films were foamed at 40 °C for 3 min. The obtained foam (with a density of ~0.38 g cm^{-3}) had an average cell size of ~400 nm and featured a nucleation efficiency of ~0.5, while for the bare nanoparticles (120 nm) the nucleation efficiency was only 0.09 (see supporting information). Hence PDMS grafting to nanoparticles seems to be a very promising strategy for enhancing the nucleation efficiency of nanoparticles in polymer foaming. In fact, upon the addition of PDMS grafted nanoparticles, foam morphologies with relevant properties are within reach via batch foaming at relatively low CO_2 saturation pressures.

The theoretical thermal conductivity (λ) of the nanocomposite PS and PMMA foams obtained in this study can be determined using a model established by Sonntag and coworkers [9] for the thermal conductivity of nanocellular PS foams. Based on this model the values of λ for the PS and PMMA foams containing PDMS grafted silica nanoparticles was estimated to be ~22.0 mW m^{-1} K^{-1} and 24.0 mW m^{-1} K^{-1}, respectively (see supporting information). These numbers are lower compared to commercially available EPS and XPS (31.0–45.0 mW m^{-1} K^{-1}) foams and can compete with existing polyurethane based foams (20–22 mW m^{-1} K^{-1}). We note that the model used resulted in thermal conductivity values that were in good agreement with reported experimentally obtained thermal conductivity values for nanocellular polyimide foams. However, more recent work reported by Rodríguez-Pérez and coworkers [11] points towards and underestimation of the thermal conductivity upon increasing cell wall thicknesses. In addition, the model used does not take into account the presence of nanoparticles in the cell walls and its effect on the solid phase thermal conductivity.

Since (meth)acrylate based polymers saturated at CO_2 pressures exceeding 250 bar provided the lowest density nanocellular foams reported until today [13], our future efforts are directed towards understanding and improving the nucleation behavior of polymer grafted nanoparticles in (meth)acrylate based polymer/CO_2 systems. In particular, the effect of particle size (*i.e.* curvature), surface roughness and the composition of the interface/interphase have our attention, since there is a lack in a quantitative understanding of the role of these parameters on cell nucleation at the macromolecular length scale. We believe that an enhanced understanding of these issues is of pivotal importance for advancing nanocellular foaming to industrially relevant foaming conditions and levels.

4. Conclusion

Silica nanoparticles grafted with low surface energy polymers were exploited as highly efficient nucleation agents in the CO_2 batch foaming of PS and PMMA. Following the synthesis of SiO_2, SiO_2-PS, SiO_2–F and SiO_2-PDMS nanoparticles with a core diameter of 80 nm, the particles were melt blended with the respective matrix polymers. Batch foaming was used to produce micro- and nanocellular foams. The obtained nanocomposite foams showed that *i*) the addition of nanoparticles was favorable for cell nucleation and that *ii*) the grafting of a thin PDMS shell to the silica nanoparticles increased the nucleation efficiency to 0.5. The obtained nucleation efficiency of PDMS grafted nanoparticles is significantly higher compared to that of other nanofillers reported so far in the open literature. Hence, PDMS grafted silica nanoparticles are very promising additives to be used as highly efficient nucleation agents for nanocellular polymer foaming. Future work should be directed towards optimization of the particle size and surface roughness as well as the thickness and composition of the low surface energy shell next to increasing our understanding of the role of these parameters on cell nucleation and foam morphology.

Acknowledgements

The authors would like to thank the MESA+ Institute for Nanotechnology of the University of Twente for financial support. Shanqiu Liu acknowledges the China Scholarship Council for funding.

Appendix A. Supplementary data

Supplementary data related to this article can be found at http://dx.doi.org/10.1016/j.polymer.2016.09.016.

References

[1] S. Costeux, CO_2-blown nanocellular foams, J. Appl. Polym. Sci. 131 (23) (2014) 41293–41308.
[2] V.P. Shastri, I. Martin, R. Langer, Macroporous polymer foams by hydrocarbon templating, Proc. Natl. Acad. Sci. U. S. A. 97 (5) (2000) 1970–1975.
[3] Y.H. Kim, S.J. Choi, J.M. Kim, M.S. Han, W.N. Kim, Effects of organoclay on the thermal insulating properties of rigid polyurethane foams blown by environmentally friendly blowing agents, Macromol. Res. 15 (7) (2007) 676–681.
[4] X. Dai, Z. Liu, Y. Wang, G. Yang, J. Xu, High damping property of microcellular polymer prepared by friendly environmental approach, J. Supercrit. Fluids 33 (3) (2005) 259–267.
[5] B. Shen, W. Zhai, M. Tao, J. Ling, W. Zheng, Lightweight multifunctional polyetherimide/graphene@Fe3O4 composite foams for shielding of electromagnetic pollution, ACS Appl. Mater. Interfaces 5 (21) (2013) 11383–11391.
[6] J. Ling, W. Zhai, W. Feng, B. Shen, J. Zhang, W. Zheng, Facile preparation of lightweight microcellular polyetherimide/graphene composite foams for electromagnetic interference shielding, ACS Appl. Mater. Interfaces 5 (7) (2013) 2677–2684.
[7] K. Rezwan, Q.Z. Chen, J.J. Blaker, A.R. Boccaccini, Biodegradable and bioactive porous polymer/inorganic composite scaffolds for bone tissue engineering, Biomaterials 27 (18) (2006) 3413–3431.
[8] D. Miller, V. Kumar, Microcellular and nanocellular solid–state polyetherimide (PEI) foams using sub–critical carbon dioxide II. Tensile and impact properties, Polymer 52 (13) (2011) 2910–2919.
[9] C. Forest, P. Chaumont, P. Cassagnau, B. Swoboda, P. Sonntag, Polymer nano–foams for insulating applications prepared from CO_2 foaming, Prog. Polym. Sci. 41 (2015) 122–145.
[10] L.W. Hrubesh, R.W. Pekala, Thermal properties of organic and inorganic aerogels, J. Mater. Res. 9 (3) (1994) 731–738.
[11] B. Notario, J. Pinto, E. Solorzano, J.A. de Saja, M. Dumon, M.A. Rodríguez–Pérez, Experimental validation of the Knudsen effect in nanocellular polymeric foams, Polymer 56 (2015) 57–67.
[12] S.S. Sundarram, L. Wei, On thermal conductivity of micro-and nanocellular polymer foams, Polym. Eng. Sci. 53 (9) (2013) 1901–1909.
[13] S. Costeux, L. Zhu, Low density thermoplastic nanofoams nucleated by nanoparticles, Polymer 54 (11) (2013) 2785–2795.
[14] H. Yokoyama, K. Sugiyama, Nanocellular structures in block copolymers with CO_2–philic blocks using CO_2 as a blowing agent: crossover from micro–to nanocellular structures with depressurization temperature, Macromolecules 38 (25) (2005) 10516–10522.
[15] Y.P. Handa, Z.Y. Zhang, A new technique for measuring retrograde vitrification in polymer–gas systems and for making ultramicrocellular foams from the retrograde phase, J. Polym. Sci. Pol. Phys. 38 (5) (2000) 716–725.
[16] J.A.R. Ruiz, M. Pedros, J.M. Tallon, M. Dumon, Micro and nano cellular amorphous polymers (PMMA, PS) in supercritical CO_2 assisted by nanostructured CO_2–philic block copolymers–One step foaming process, J. Supercrit. Fluids 58 (1) (2011) 168–176.
[17] C. Zeng, X. Han, L.J. Lee, K.W. Koelling, D.L. Tomasko, Polymer–clay nanocomposite foams prepared using carbon dioxide, Adv. Mater 15 (20) (2003) 1743–1747.
[18] B. Krause, R. Mettinkhof, N.F.A. van der Vegt, M. Wessling, Microcellular foaming of amorphous high–T_g polymers using carbon dioxide, Macromolecules 34 (4) (2001) 874–884.
[19] B. Krause, K. Diekmann, N.F.A. van der Vegt, M. Wessling, Open nanoporous morphologies from polymeric blends by carbon dioxide foaming, Macromolecules 35 (5) (2002) 1738–1745.
[20] L. Chen, D. Rende, L. Schadler, R. Ozisik, Polymer nanocomposite foams, J. Mater. Chem. A 1 (12) (2013) 3837–3850.
[21] S. Liu, J. Duvigneau, G.J. Vancso, Nanocellular polymer foams as promising high performance thermal insulation materials, Eur. Polym. J. 65 (2015) 33–45.
[22] J. Lothe, G.M. Pound, in: A.C. Zettlemoyer (Ed.), Nucleation, Chapter 3, Marcel

Dekker, New York, 1969.
[23] D.W. Oxtoby, Density functional methods in the statistical mechanics of materials, Annu. Rev. Mater. Res. 32 (1) (2002) 39–52.
[24] P. Spitael, C.W. Macosko, R.B. McClurg, Block copolymer micelles for nucleation of microcellular thermoplastic foams, Macromolecules 37 (18) (2004) 6874–6882.
[25] L. Li, T. Nemoto, K. Sugiyama, H. Yokoyama, CO_2 foaming in thin films of block copolymer containing fluorinated blocks, Macromolecules 39 (14) (2006) 4746–4755.
[26] J. Pinto, M. Dumon, M. Pedros, J. Reglero, M.A. Rodriguez–Perez, Nanocellular CO_2 foaming of PMMA assisted by block copolymer nanostructuration, Chem. Eng. J. 243 (2014) 428–435.
[27] S. Bärwinkel, R. Bahrami, T.I. Löbling, H. Schmalz, A.H.E. Müller, V. Altstädt, Polymer foams made of immiscible polymer blends compatibilized by Janus particles–effect of compatibilization on foam morphology, Adv. Eng. Mater 18 (5) (2016) 814–825.
[28] M. Okamoto, P.H. Nam, P. Maiti, T. Kotaka, T. Nakayama, M. Takada, M. Ohshima, A. Usuki, N. Hasegawa, H. Okamoto, Biaxial flow–induced alignment of silicate layers in polypropylene/clay nanocomposite foam, Nano Lett. 1 (9) (2001) 503–505.
[29] J. Shen, C. Zeng, L. Lee, Synthesis of polystyrene–carbon nanofibers nanocomposite foams, Polymer 46 (14) (2005) 5218–5224.
[30] X. Cao, L.J. Lee, T. Widya, C. Macosko, Polyurethane/clay nanocomposites foams: processing, structure and properties, Polymer 46 (3) (2005) 775–783.
[31] S. Siripurapu, J.M. DeSimone, S.A. Khan, R.J. Spontak, Controlled foaming of polymer films through restricted surface diffusion and the addition of nanosilica particles or CO_2–philic surfactants, Macromolecules 38 (6) (2005) 2271–2280.
[32] L.J. Lee, C. Zeng, X. Cao, X. Han, J. Shen, G. Xu, Polymer nanocomposite foams, Compos. Sci. Technol. 65 (15) (2005) 2344–2363.
[33] W. Zhai, J. Yu, L. Wu, W. Ma, J. He, Heterogeneous nucleation uniformizing cell size distribution in microcellular nanocomposites foams, Polymer 47 (21) (2006) 7580–7589.
[34] K. Goren, L. Chen, L.S. Schadler, R. Ozisik, Influence of nanoparticle surface chemistry and size on supercritical carbon dioxide processed nanocomposite foam morphology, J. Supercrit. Fluids 51 (3) (2010) 420–427.
[35] S. Siripurapu, J.M. DeSimone, S.A. Khan, R.J. Spontak, Low-temperature, surface-mediated foaming of polymer films, Adv. Mater 16 (12) (2004) 989–994.
[36] L. Chen, R. Ozisik, L.S. Schadler, The influence of carbon nanotube aspect ratio on the foam morphology of MWNT/PMMA nanocomposite foams, Polymer 51 (11) (2010) 2368–2375.
[37] G. Harikrishnan, I.L. Chris, M.A. Arunagirinathan, C.W. Macosko, Probing nanodispersions of clays for reactive foaming, ACS Appl. Mater. Interfaces 1 (9) (2009) 1913–1918.
[38] J. Yang, Y. Sang, F. Chen, Z. Fei, M. Zhong, Synthesis of silica particles grafted with poly (ionic liquid) and their nucleation effect on microcellular foaming of polystyrene using supercritical carbon dioxide, J. Supercrit. Fluids 62 (2012) 197–203.
[39] J. Yang, L. Huang, Y. Zhang, F. Chen, M. Zhong, Mesoporous silica particles grafted with polystyrene brushes as a nucleation agent for polystyrene supercritical carbon dioxide foaming, J. Appl. Polym. Sci. 130 (6) (2013) 4308–4317.
[40] J.R. Dann, Forces involved in the adhesive process: I. Critical surface tensions of polymeric solids as determined with polar liquids, J. Colloid Interf. Sci. 32 (2) (1970) 302–320.
[41] S. Wu, Calculation of interfacial tension in polymer systems, J. Polym. Sci. Part C. Polym. Symp. 34 (1) (1971) 19–30.
[42] V. Kumar, N.P. Suh, A process for making microcellular thermoplastic parts, Polym. Eng. Sci. 30 (20) (1990) 1323–1329.
[43] M. Svetozar, N. Filipović–Vinceković, L. Sekovanić, Precipitation of amorphous SiO_2 particles and their properties, Braz. J. Chem. Eng. 28 (1) (2011) 89–94.
[44] H. Kim, H.G. Kim, S. Kim, S.S. Kim, PDMS–silica composite membranes with silane coupling for propylene separation, J. Membr. Sci. 344 (1) (2009) 211–218.
[45] S. Radice, E.D. Dedda, C. Tonelli, R.D. Pergola, A. Milani, C. Castiglioni, FT–IR spectroscopy and DFT calculations on fluorinated macromer diols: IR intensity and association properties, J. Phys. Chem. B 114 (19) (2010) 6332–6336.
[46] P. Gong, M. Ohshima, Effect of interfacial tension on the cell structure of poly(methyl methacrylate)/bisphenol A polycarbonate blends foamed with CO_2, J. Appl. Polym. Sci. 131 (5) (2014) 39228–39239.